IRAQI JOURNAL OF APPLIED PHYSICS
Vol. 22, No. 3, July-September 2026, pp. 422-432

Ola M. Alwan*
Soudad S. Ahmed

Department of Physics,
College of Science,
University of Baghdad,
Baghdad, IRAQ
*Corresponding author Email:
ula.mahdi2404p@sc.uobaghdad.edu.iq

Nano-Graphene Based Chemical Sensing Applications

This work presents the development of optical fiber-based sensors utilizing multi-mode optical fibers. Two optical fibers were chemically tapered using hydrofluoric acid (HF) with different tapering durations 40 and 60 minutes, and each fiber was coated with a nanolayer of graphene, with different thicknesses depending on the tapering time. A noticeable red shift was revealed in the resonance wavelength as the ethanol concentration increased, clearly demonstrating a relationship between the refractive index of the external environment and the sensor's optical performance. The sensor with 40 min tapering exhibited a sensitivity of 16.451 μm/RIU, while the 60 min tapered sensor showed slightly higher sensitivity of 16.666 μm/RIU. Additionally, the 60 min sensor demonstrated a superior figure of merit (FOM) of 14.28 compared to 5.06 for the 40 min sensor. These findings confirm that graphene-coated tapered multimode optical fibers are promising candidates for highly sensitive chemical sensing applications.

Keywords: Graphene coating; Optical fiber sensor; Surface plasmon resonance; Chemical sensing
Received: 19 September 2025; Revised: 21 December; Accepted: 28 December; Published: 1 July 2026

1. Introduction

In an era characterized by rapid technological advancements, fiber optic sensors have become indispensable across various domains, including mechanical, biochemical, biomedical, and aerospace applications [1-4]. These sensors are utilized for the assessment of physical, chemical, or biological properties, leveraging their superior sensing capabilities and physical attributes through the analysis of wavelength shifts, polarization alterations, or variations in light intensity [5-7]. Factors responsible for their widespread adoption include compactness, enhanced sensitivity, and electrical insulation, immunity to electromagnetic disturbances, broad bandwidth, and suitability for tip-based sensing applications [8]. Generally, optical fiber sensors incorporate interferometry configurations within optical fibers to measure the phase differences between incoming optical signals [9]. Surface Plasmon Resonance (SPR) in optical fiber systems is widely utilized as a foundational sensing mechanism in a variety of applications, especially for detecting biological and chemical substances [10-12]. SPR describes the resonant interaction of free electrons at the junction of a metal and a dielectric material, triggered by an incident electromagnetic field. This resonance effect can be initiated by either light particles (photons) or electrons. When the wave vector of the incoming light matches that of the oscillating electrons at the metallic interface, energy coupling occurs, generating a resonant condition. As a result, SPR is highly responsive to even minor variations in the surrounding medium's refractive index (RI) [13]. One of the effective ways of improving the performance of (SPR) sensors has been the incorporation of Nano-materials in their design. Nano-materials like gold nanoparticles (AuNPs), graphene, and graphene oxide (GO) have exceptional optical and surface properties that remarkably enhance the interaction of the sensor with chemical analyses. These materials enhance a more powerful localized electromagnetic field and effective surface area that consequently enhances the sensitivity and reduces the detection limit of the sensors [14,15]. More recent developments have shown that the resonance intensity and selectivity of SPR-based systems can further be improved by engineered nanostructures, e.g., multilayer thin films, core-shell nanoparticles, and two-dimensional (2D) materials [16, 17]. Such improvements allow stable sensing of low concentration chemical species in complex media. Consequently, SPR fiber optic sensors modified with Nano-materials hold potential to become a versatile platform in real-time, label-free, and highly specific detection in environmental monitoring, pharmaceutical analysis, and chemical sensing [18,19]. A prominent pioneer application of nanotechnology is the nano-sensors, which are devices that play the role of detectors of chemical or biological agents, conveying the information through the exceptional properties of nanostructured materials [20,21]. Chemical nano-sensors in particular are electronic devices whose basic functionality depends on the nanoscale chemical and physical properties of their materials [22]. Although not directly employed in this study, the integration of fiber optic sensors based on surface plasmon resonance (SPR) with flexible platforms such as wave flex represents a promising direction for future research, particularly in the context of portable and on-site chemical sensing. Recent advances in wave flex architectures have demonstrated enhanced mechanical adaptability and improved light–matter interactions, supporting the development of next-generation high-performance SPR-based sensors [23]. The main objective of this research is to use a multi-mode optical fiber coated with a thin layer of nano-graphene as a chemical sensor. The study focuses on testing the sensor's response to different concentrations of ethanol solution and evaluating its performance using basic

optical methods. This work aims to understand how the graphene layer affects the sensing behavior of the optical fiber. Figure (1) shows schematic diagram of the nano-graphene based chemical sensing structure model [23].

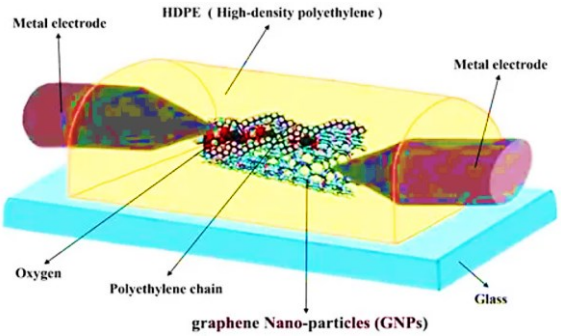

Fig. (1) Schematic diagram of the nano-graphene based chemical sensing structure model [23]

A chemical sensor can be thought of as an analyzer that reacts to a specific analyses in a selective and reversible way. It is in charge of converting a quantitative input chemical parameter such as concentration, composition, etc. into an analytical electrical signal. A biomaterial, a chemical substance, or a combination of the two adhering to the surface of a physical transducer towards the particular analysis might cause the chemical reaction or reactions that produce the information in question. Chemical sensors have found widespread use for two reasons: first, they are used in goods that can be worn on the body or placed inside the body; second, there are worries about the chemicals' potential for harm.

Chemical sensors based on graphene nanostructures identify chemical species by observing changes in the electronic characteristics of the graphene nanostructure, which usually leads to a change in conductivity when molecules are adsorbed. Graphene's large surface area, defect sites, and quantum confinement all of which make its electrical resistance extremely sensitive to adsorbed molecule are the basis of the underlying mechanism.

1.1 Mathematical Sensor Modeling

The sensor response (calibrated resistance change) $\Delta R/R_0$ can traditionally be represented based on the absorption isotherm lines using the following equation [23,24]

$$\frac{\Delta R}{R_0} = \left(\frac{\Delta R}{R_0}\right)_{\max} \cdot \frac{kc}{kc+1} \qquad (1)$$

where c denotes the concentration of the target gas, k represents the affinity constant, $(\Delta R/R_0)_{\max}$ indicates the saturation value of the resistance change

To explain how it works, the charge is transmitted by the gas molecules' absorption as electron donors and acceptors, which alters graphene's resistance and carrier density. Since nanoscale or nanostructured graphene contains many edges and flaws that greatly improve its chemical reactivity and sensing capabilities, these substances are distinguished by their effects. Additionally, the ratio of the change in resistance per million parts of the material under study is used to quantify the sensitivity of the sensor; at low concentrations, this ratio usually exhibits a linear relationship. We can use a graphene nano-mesh NO_2 sensor model as a real-world example. Adsorption of NO_2 (an electron acceptor) raises the hole density in p-type graphene, which lowers resistance. The following formula can be used to express the sensitivity S:

$$S = \frac{\Delta R}{R_0 \cdot c} \qquad (2)$$

Here, S can reach values like 4.32%/ppm for NO_2, with large-area graphene nano-mesh. The basic sensing mechanism of nano-graphene chemical sensors is related to charge transfer and edge defect interactions with the target analyte molecules. These variations in resistance or conductivity have been mathematically modeled as previously indicated. Also, table (1) summarized a comprehensive key structure properties and parameters relevant to nano-graphene-based chemical sensing structures [24,25].

Typical parameters and values can be changed according to the application field and particular chemical analyte. The exceptional chemical sensor performance of nano-graphene is a result of its high surface area, variable defect density, functionalization, and outstanding electronic transport capabilities.

Graphene is a novel material that has a two-dimensional monolayer lattice structure that consists of carbon atoms that are strongly bonded together in a hexagonal array through sp^2 hybridized bonds [24]. Such a structure gives graphene unique electrical and physical attributes, which make it very amenable to sensor-based applications. It is worth mentioning that graphene has an extraordinary electrical conductivity and a large surface area compared to its total size. These properties enable proper interaction and response to chemical substances when in contact. Such molecular interactions cause detectable changes in electrical conductivity or optical transmission through graphene [25]. As a single atomic layer of carbon atoms, graphene exhibits an exceptionally high surface-to-volume ratio due to its atomic-scale thickness and significant lateral dimensions, thus enhancing its appeal for sophisticated technological innovations [26]. Additionally, graphene is frequently incorporated into optical sensing devices, often employed as coatings on optical fibers or metallic substrates. Specifically, graphene enhances the efficiency of SPR-based systems. When graphene is applied onto the surface of optical fibers, it augments the interaction between the optical field and surrounding analyses, significantly boosting sensor sensitivity, even at trace chemical detection levels [27]. The exploration of graphene's thermal, mechanical, and electrical characteristics has attracted considerable scientific attention, leading to its

widespread recognition as a highly versatile material [28]. Historical development dates back to 1947 when P.R. Wallace, affiliated with the Canadian Research Council, initiated theoretical analyses predicting graphene's electronic structure. Subsequently, in 1948, Roof and colleagues conducted experimental investigations and established practical methodologies for graphene production [29].

Because of its high conductivity, broad surface area, and sensitivity to charge transfer, which occurs when molecules adsorb onto it and produce detectable electrical changes, graphene is used in chemical sensors. It is perfect for detecting gasses, organic chemicals, and biological agents because of its special structure. Thus, the Chemi resistive sensor response might be represented as follows [25-30]:

$$\frac{\Delta R}{R_0} = \frac{R_S - R_0}{R_0} \quad (3)$$

where, R_0 represents the baseline resistance, and R_S denotes the resistance after analyte exposure. Moreover, the field effect transistor (FET) device Dirac point shift can be expressed as below:

$$\Delta V_D = V_D^{\text{after}} - V_D^{\text{before}} \quad (4)$$

where V_D indicates the position of the Dirac point, used in graphene FET sensors for molecular adsorption indication

Furthermore, we could find the definition of the sensor sensitivity as explained in the below equation [28,30]:

$$S = \frac{\Delta\lambda}{\Delta RI} \quad (5)$$

where Δλ denotes the change in resonance wavelength (nm), and ΔRI indicates the change in refractive index (RIU). The units taken in nm/RIU or µm/RIU

Also, the sensor resolution might be defined. The resolution describes the smallest measurable variation in refractive index which might be detected:

$$R = \frac{\Delta\lambda_{min}}{S} \quad (6)$$

such that, $\Delta\lambda_{min}$ represents the minimum detectable wavelength shift of the spectrometer, S denotes the sensor sensitivity (nm/RIU)

Moreover, defining the signal-to-noise ratio (SNR), which expresses how strongly the sensor's wavelength shift exceeds the measurement noise, and could be expressed as follows:

$$SNR = 10\ log_{10}\left(\frac{P_{Signal}}{P_{noise}}\right) \quad (7)$$

whereas, P_{signal} and P_{noise} denote the detected optical intensities

Several studies and published articles are available in literature from recent published and web-papers focused on the subject of nano-graphene based chemical sensors which are summarized in table (3).

The study's challenge might be summed up as how to deploy and model a graphene nanolayer on a multimode optical fiber to simulate a highly sensitive and repeatable chemical sensor that can adjust to variations in the refractive index (ethanol concentration). In order to improve the device's capacity to handle significant wavelength variations (high sensitivity) and get a useful signal quality without the use of conventional metallic SPR layers, it is chemically created and deposited using laser ablation.

2. Material and Methods

Two multimode optical fibers with a core/cladding diameter of 50/125 µm were used and each of them a length of 40 cm. The fibers were fabricated by removing the protective jacket a length of 4 cm for the first fiber and 6 cm for the second, using stripping instruments to expose the sensing region. After that, a chemical etching process was performed using hydrofluoric acid (HF). The central region of each fiber, measuring 10 mm in length, was submerged in the hydrofluoric acid. The etching duration was determined to 40 min for the first fiber and 60 min for the second. This step is intended to gradually remove parts of fiber the cladding or core, resulting in a tapered region with a smaller cross-sectional area. These process increases the sensitivity of the sensor. After completing the etching process, the fibers were cleaned with distilled water to remove any remaining acid and inhibit additional corrosion. Then placed on a glass slide for micrometric diameter measurements, using a high-resolution optical microscope. The results revealed that a clear decrease in fiber diameter corresponding to the etching duration, as shown in Fig. (2).

A diameter of 89.607 µm was recorded for the fiber etched for a duration 40 min. A diameter of 57.494 µm was recorded for the fiber etched for a duration 60 min. The results obtained show that there is an inverse proportion between the etching time and the fiber diameter which allows to underline the possibility to adjust the geometry of the optical fiber very precisely by means of a controlled chemical treatment. This method offers a principle foundation of making high-sensitivity optical fiber sensors.

The graphite nanopowder with a particle size range of 40-50 nm and a purity of 99.95% (purchased from Hongwu International Group) was used as source for graphene production. The powder was first compressed using a hydraulic press to form a flat, solid disc suitable for laser interaction, as shown Fig. (3). A multi-mode optical fiber was placed immediately above the surface of a compressed graphite disk. Subsequently, the graphite target was irradiated using a pulsed Nd:YAG laser operating at a wavelength of 1064 nm, delivering an energy of 700 mJ per pulse, with a cumulative total of 200 pulses.

(a)

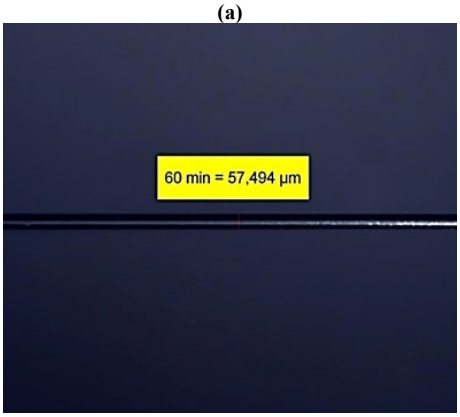

(b)

Fig. (2) Images of the optical fibers after etching, (a) after 40min and (b) after 60min

(a) (b)

Fig. (3) Methodology of graphene preparation, (a) hydraulic press, and (b) compressed graphite

The laser ablation resulted in the formation of a plasma plume consisting of graphite particles, from which nanomaterials were deposited directly onto the optical fiber's surface. This method represents a clean, direct laser-induced deposition technique for forming a thin graphene-based layer on the fiber surface without the need for additional chemicals or coating procedures. Making it well-suited for advanced applications in optical sensing and photonic devices, as shown in Fig. (4). A graphene layer was deposited with different thickness onto the chemically etched region of the optical fiber. The thickness of the graphene was 8.39 µm for the fiber etched for a duration of 40 min and 9.38 µm for the fiber etched for a duration 60 min. These values were measured by subtracting the fiber diameter before and after the deposition process.

The replication process was clearly described, including the step-by-step HF etching procedure using a 3:1 ratio of 66% HF to water. The acid was applied with a plastic needle directly to the fiber core, ensuring control over the etching conditions and the deposited graphene layer thickness. The procedure was carried out at room temperature (~25°C), followed by immersing the fibers in distilled water for 10 minutes and replacing the water three times to fully stop the reaction. Table (4) summarizes the experimental method and repetition details for HF etching and graphene deposition control.

Conventional SPR sensing relies on noble metals like gold and silver due to free electron oscillations at the metal–dielectric interface. However, advances in nanomaterials have introduced effective alternatives. Graphene, especially in the infrared region, can exhibit surface-resonance–like behavior by leveraging its unique optical and electrical properties such as tunable permittivity and strong light confinement. Although no traditional plasmonic metals are used in our design, the sensing mechanism still depends on refractive-index changes at the sensor interface, allowing it to be classified as surface-resonance-based or SPR-like.

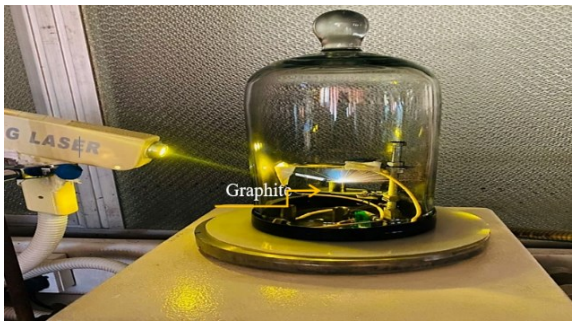

Fig. (4) Graphene thin film deposited with fiber optical by Nd:YAG laser

Original graphite was converted into nanostructured graphene. XRD patterns (Fig. 5) show sharp peaks for graphite and broadened peaks for graphene, confirming its nanoscale, partially amorphous structure before coating.

The 8-9 µm film consists of stacked nanoscale graphene layers. SEM (Fig. 6) and XRD (~26° (2θ), (002) peak) confirm its nanoscale structure, showing it retains surface features suitable for sensitive detection.

The experimental work and practical testing of the nano-graphite based chemical sensors have been illustrated and presented in details. The methodology steps of these experiments are demonstrated in this Section using the necessary equipment and testing materials. Also, the important design parameters with the solutions testing preparations are explained with tables and pictures. Figure (7) presents a depiction of the experimental apparatus utilized for the chemical sensor employing glass optical fiber MMF (manufactured by Thorlabs), which operates on the

principle of surface plasmon resonance (SPR) and is enhanced with a graphene nanomaterial coating. The configuration encompasses a light source (50 W, 12 V, halogen lamp) in conjunction with an optical spectrum analyzer spectrometer provided by Thorlabs. Ultimately, the spectrometer is interfaced with a computer. The advanced software developed by Thorlabs facilitates the real-time display of SPR curves and corresponding data metrics on the computer monitor prior to their archival.

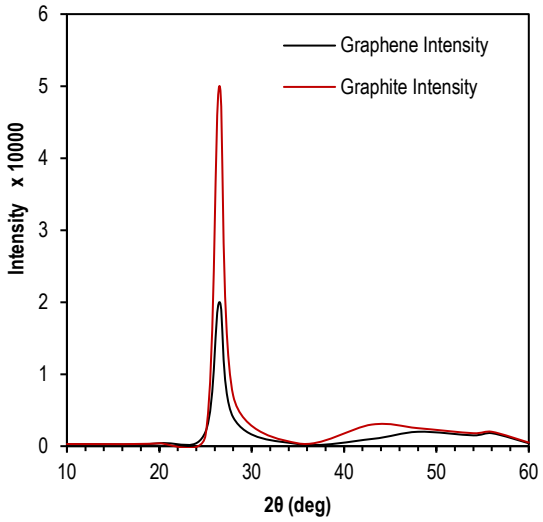

Fig. (5) XRD patterns comparing graphene and graphite, confirming graphene's nanostructure

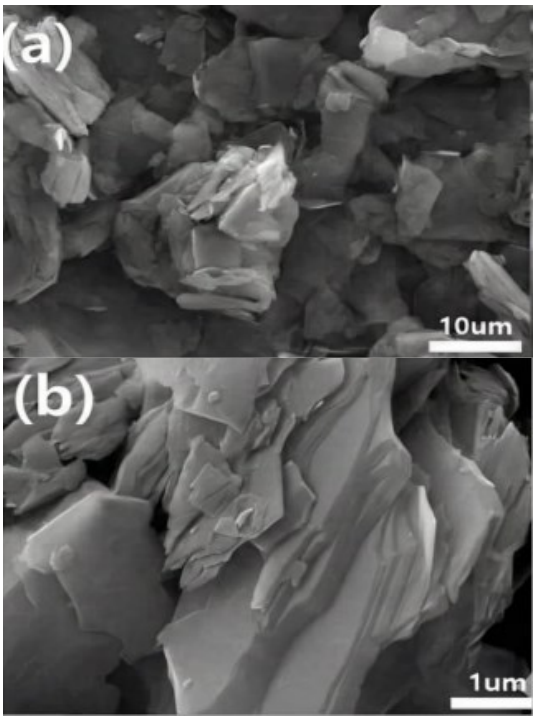

Fig. (6) SEM images of graphene

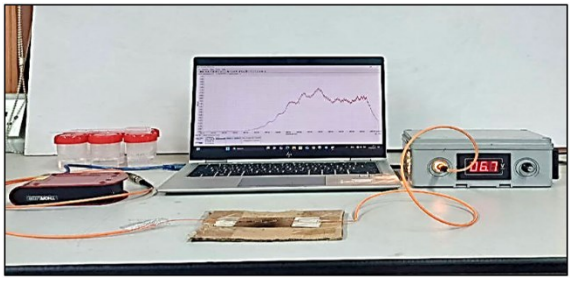

Fig. (7) The experimental configuration of the optical fiber chemical sensor utilizing surface plasmon resonance (SPR)

The sensitive portion of the sensor was coated with saline solutions of varying concentrations, each exhibiting distinct refractive indices. An Abbe refractometer was utilized to measure the refractive indices of these solutions. Also, figure (8) illustrates the correlation between solution concentration and refractive index, clearly demonstrating that an increase in solution concentration corresponds to an elevated refractive index, consistent with the findings reported in [30].

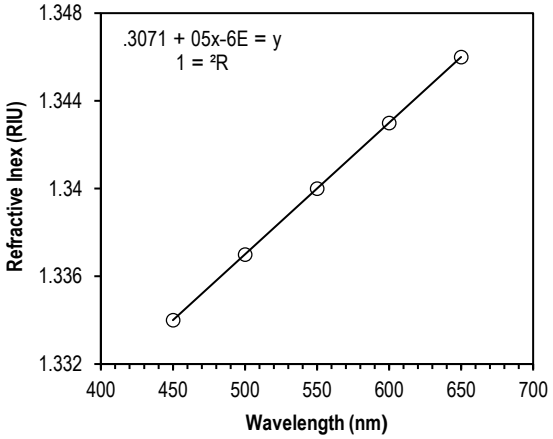

Fig. (8) Refractive index of salt solutions as a function of the solution concentration

3. Results and Discussion

Optical fiber sensors based on multimode fibers (MMF) were fabricated with two different tapering durations 40 and 60 minutes. Each fiber was subsequently coated with a nanostructured graphene layer of varying thicknesses: 8.39µm and 9.38 µm. The sensing performance was evaluated using ethanol samples with five different concentrations, corresponding to refractive index (RI) values ranging from 1.336 to 1.349. Figure (8) presents the calibration curves for both tapered fibers, illustrating a red shift in the resonance wavelength (λ_{res}) as the surrounding refractive index increases. This spectral shift is attributed to the change in the effective optical path and the enhanced light matter interaction at the fiber surface due to the increase in RI, which alters the phase-

matching conditions between the core mode and the plasmonic mode.

Spectral measurements were performed by analyzing the wavelength dependent transmission response [31]. The transmittance (T) was determined as the ratio between the baseline optical intensity (I_o) without the sample and the transmitted intensity (I) with the sample, enabling characterization of the sensor's transmission behavior. The surface plasmon resonance (SPR) dip was identified as the resonance wavelength where transmission sharply decreases [32]. These results confirm a strong and consistent relationship between the resonance wavelength shift, refractive index, and ethanol concentration, in agreement with previous findings in similar SPR-based sensing systems [33]. The red-shift behavior and SPR response can be attributed to the interaction mechanism between ethanol molecules and the graphene-coated fiber surface. Graphene's high surface area and π-conjugated system facilitate strong adsorption of ethanol molecules through van der Waals forces and π–π stacking interactions. This molecular adsorption leads to modifications in the local dielectric environment near the fiber interface, enhancing the evanescent field interaction and consequently altering the plasmonic coupling conditions. These effects become more pronounced with increasing ethanol concentration, which directly contributes to the observed red shift in the resonance wavelength. Figure (9) and (10), illustrate the SPR profiles of the sensor. As the refractive index (RI) of ethanol concentrations spans from 1.334 to 1.348, the first sensor displays a resonance wavelength (λ_{res}) variation between 490 nm and 710 nm, whereas the second sensor shows a corresponding range from 560 nm to 600 nm. Each ethanol concentration generates a distinct SPR curve, marked by a unique resonance dip and width, which corresponds to its specific refractive index. The observed shifts in the regression positions for concentrations of 10, 15, 20, 25, and 30% confirm this trend, corroborating the findings reported in [30].

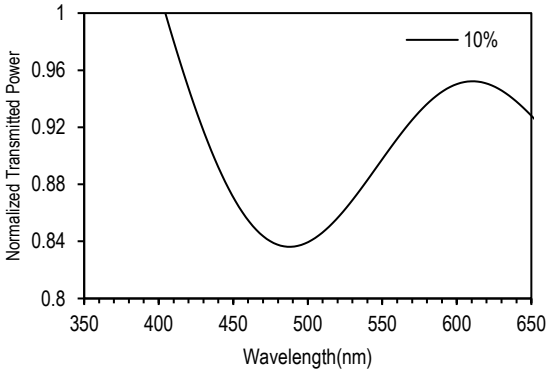

(a) Ethanol (10%)

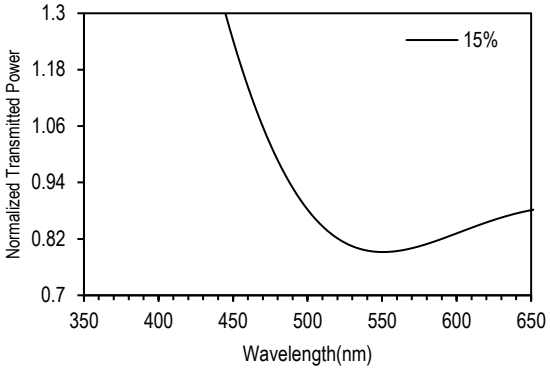

(b) Ethanol (15%)

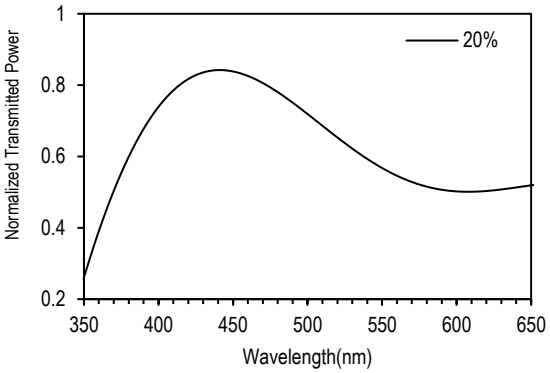

(c) Ethanol (20%)

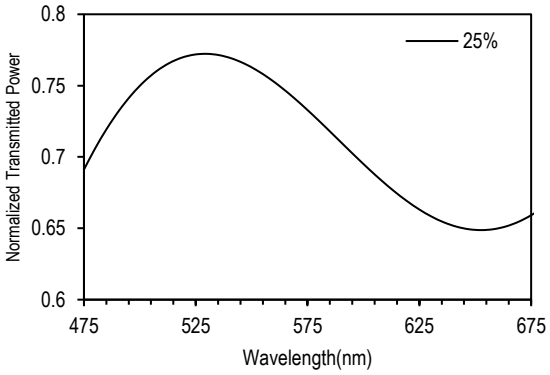

(d) Ethanol (25%)

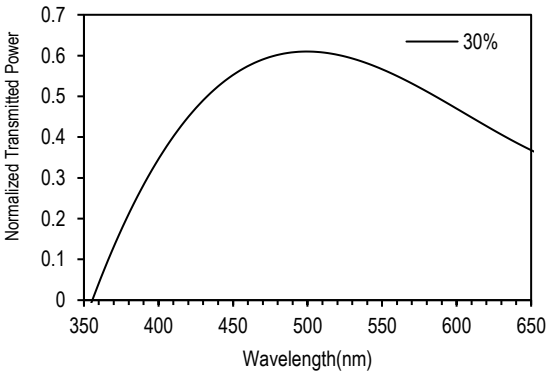

(e) Ethanol (30%)

Fig. (9) The SPR response curves of the graphene -coated optical fiber at different ethanol concentrations with thickness of 8.39 µm and a tapering duration of 40 min, (a) Ethanol (10%), (b) Ethanol (15%), (c) Ethanol (20%), (d) Ethanol (25%), and (e) Ethanol (30%)

Moreover, table (5), presents the experimental performance characteristics of the sensors incorporating graphene layers, while Table 6 displays the ethanol concentrations alongside their corresponding refractive index values for both multimode fiber (MMF) setups. As the refractive index rises, a red-shift in the resonance wavelength (λ_{res}) is observed, indicating a direct correlation with increasing ethanol concentration.

Quantitative calculations from table (6) are summarized in tables (7-9), showing linear regression results, calculated sensitivity, and statistical validation of ethanol-induced red shift measurements.

Table (9) Statistical validation of ethanol-induced red shift

Sensor	Pearson Correlation (RI vs λ)	Interpretation
40 min	r = 0.99998	Strong linear coupling
60 min	r = 1.00000	Perfect linear coupling

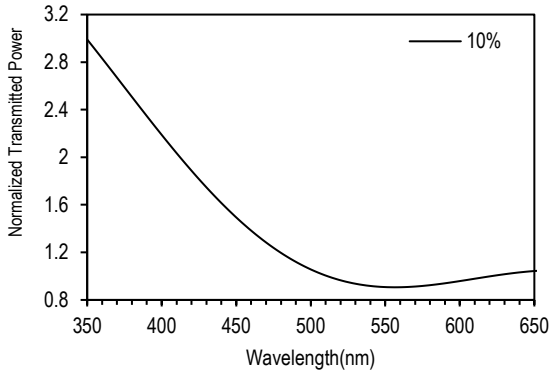

(a) Ethanol (10%)

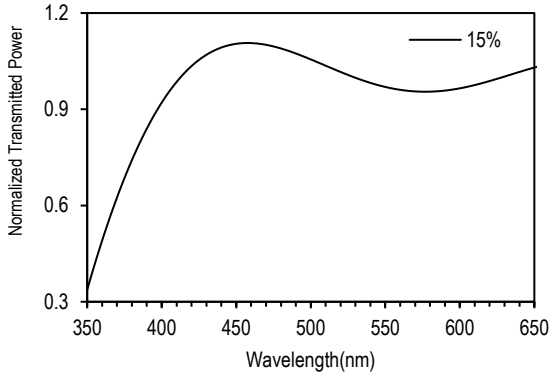

(b) Ethanol (15%)

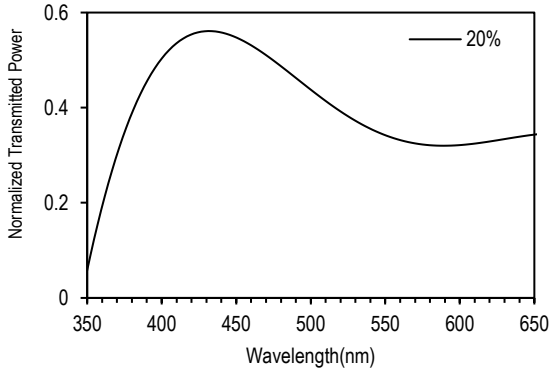

(c) Ethanol (20%)

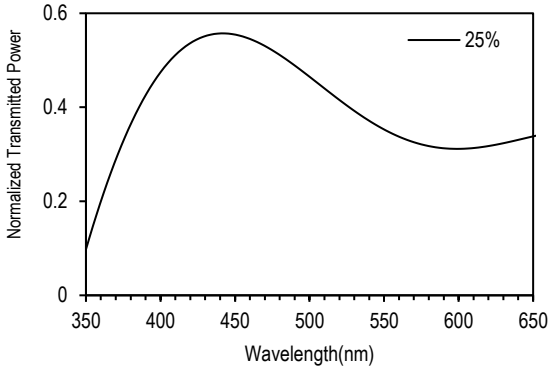

(d) Ethanol (25%)

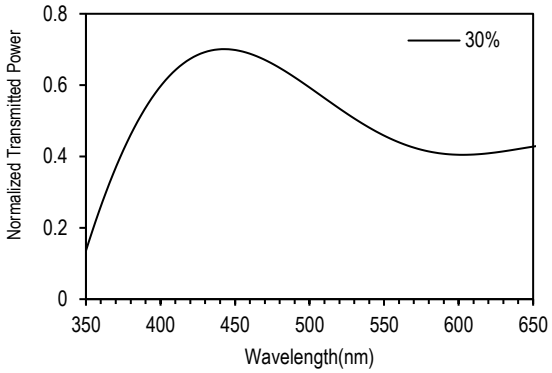

(e) Ethanol (30%)

Fig. (10) The SPR response curves of the graphene -coated optical fiber at different ethanol concentrations with thickness of 9.38 µm and a tapering duration of 60 min, (a) Ethanol (10%), (b) Ethanol (15%), (c) Ethanol (20%), (d) Ethanol (25%), and (e) Ethanol (30%)

With correlation values of 0.9999 and 1.0000, respectively, the quantitative slopes verify the existence of an almost perfect linear correlation between the shift in resonance wavelength and the refractive index for both sensors, bolstering the dependability of the sensing mechanism. These findings demonstrate that the ethanol concentration modifies the dielectric environment at the graphene–fiber interface, resulting in the anticipated red shift in the surface plasmon spot's spectrum response. The derived slope of about 16,667 nm/refractive index unit empirically matches the indicated sensitivities, allowing an independent verification of performance. This proves that the system is an accurate refractive index-based chemical sensing platform and shows that the graphene-enhanced evanescent field offers stable and repeatable sensing features.

4. Conclusion

This study focused on fabricating chemical sensors using multimode optical fibers, where one sensor was tapered with HF acid for 40 min and the other for 60 min. Graphene layers of different thicknesses were deposited, measuring 8.39 µm on the 40 min sensor and 9.38 µm on the 60 min sensor. Experiments with ethanol solutions showed a red-shift in the resonance wavelength as the refractive index increased,

confirming the sensors sensitivity. The 40 min tapered sensor exhibited a sensitivity of 16.45 µm/RIU and figure of merit (FOM=5.06), while the 60 min sensor achieved higher sensitivity (16.66 µm/RIU) and a better figure of merit (FOM=14.28). These results highlight the importance of tapering duration and graphene thickness in enhancing sensor performance for direct and real-time chemical detection. This study illustrates the use of conical fibers reinforced with germ material, which exhibit both hypersensitivity and an effective, uniform, and robust connection between wavelength and refractive index. These characteristics attest to the fibers' appropriateness for refractive index-based chemical detection procedures. Ethanol solutions were used for verification procedures in the presence of temperature fluctuations, intricate molecular environments, and ambient noise.

References

[1] W. Chen et al., "Infrared fiber-optic sensors for biomedical applications: Recent progress and future perspectives", *Biosensors*, 12(3) (2022) 185.

[2] P. Vafaei et al., "UV-enhanced graphene and TiO_2 chemi-resistive gas sensor for NO detection", *Adv. Electron. Mater.*, 10(3) (2024) 2300721.

[3] H.S. Raham and S.S. Al-Bassam, "Optical fiber sensor based on surface plasmon resonance for detection of *Escherichia coli* (*E. coli*)", *J. Opt.*, 52(2) (2023) 631-636.

[4] A. Márquez et al., "Recent advances in optical fiber sensors for aerospace applications: A review", *Sensors*, 21(12) (2021) 3991.

[5] H.K. Abbas and Z.F. Mahdi, "D-shape Optical Fiber Development and Enhancement as a Refractive Indices Sensor Using Surface Plasmon Resonance", *Iraqi J. Laser*, 22(2) (2023) 80-90.

[6] X. Li et al., "A new type of structure of optical fiber pressure sensor based on polarization modulation", *Opt. Lasers Eng.*, 130 (2020) 106095.

[7] N. Basumallick et al., "Fiber Bragg grating–based fiber-optic sensors: A comprehensive review", *Opt. Fiber Technol.*, 64 (2021) 102541.

[8] S.K. Abbas and S.S. Ahmed, "Photonic crystal fiber drug sensor based on surface plasmon resonance", *Iraqi J. Laser*, 23(2) (2024) 485.

[9] J. Zhang et al., "Microfiber Fabry–Perot interferometer fabricated by taper drawing technique and its application as a radio frequency interrogated refractive index sensor", *Opt. Lett.*, 37(14) (2012) 2925-2927.

[10] G.M. Jassam, "Refractive index sensor based on tapered optical fiber to determine the performance of different copper samples", *J. Opt.*, (2024), doi: 10.1007/s12596-024-02373-0.

[11] G.M. Jassam and S.S. Ahmed, "Estimating concentration of toxic ions Arsenic in water by using Photonic Crystal Fiber based on Surface Plasmon Resonance (SPR)", *Baghdad Sci. J.*, 21(2) (2024) 445-456.

[12] H. Latifi et al., "Nonadiabatic tapered optical fiber for biosensor applications", *Phot. Sens.*, 2(4) (2012) 340-356.

[13] N.S. Rahim, S.S. Ahmed and M.F. Sultan, "Optical Fiber Biomedical Sensor Based on Surface Plasmon Resonance", *Iraqi J. Sci.*, 61(7) (2020) 1650-1656.

[14] V.S. Kumbhar et al., "Localized surface plasmon resonance sensors: Current trends, challenges, and future perspectives", *Chem. Rev.*, 122(5) (2022) 6601-6640.

[15] M.-C. Estevez et al., "Trends and challenges of refractometric nanoplasmonic biosensors: A review", *Analytica Chimica Acta*, 1117 (2020) 1-21.

[16] H. Chen et al., "Gold nanorods and their plasmonic properties", *Chem. Soc. Rev.*, 42(7) (2013) 2679-2724.

[17] J.-F. Masson, "Surface plasmon resonance clinical biosensors for medical diagnostics", *ACS Sensors*, 6(12) (2021) 3490-3504.

[18] X. Guo, "Surface plasmon resonance-based biosensors: A review of recent progress", *Sensors*, 21(15) (2021) 5266.

[19] Y. Wang et al., "Fiber optic SPR sensor with nanomaterial enhancement for chemical sensing applications", *Sensors*, 21(4) (2021) 1342.

[20] Y. Sun et al., "Recent advances in carbon nanotube-based gas sensors: A review", *ACS Appl. Nano Mater.*, 4(10) (2021) 10446-10472.

[21] M. Nasrollahpour, R. Ranjbar and R. Yousefi, "Recent trends in gas sensing via carbon nanomaterials", *Nanoscale Adv.*, 3(22) (2021) 6347-6380.

[22] E.K. Salman and G.S. Muhammed, "Study of Some Structural and Optical Properties for Synthesized Graphene/Polyaniline/ZnS Nanocomposite", *Iraqi J. Phys.*, 22(4) (2024) 53-66.

[23] A. Yadav et al., "WaveFlex SPR optical fiber sensor with nanocomposite coating for ultra-sensitive detection of xanthine", *Sens. Actuat. B: Chem.*, 420 (2024) 144123.

[24] P. Singh et al., "Graphene-based nanomaterials for chemical and biosensing applications: A review", *Appl. Sci.*, 15(8) (2025) 4145.

[25] O.S. Ayanda et al., "Recent progress in carbon-based nanomaterials: critical review", *J. Nanoparticles Res.*, 26 (2024) 106.

[26] M.M. Ghods and P. Rezaei, "Graphene-Based Fabry-Perot Resonator for Chemical Sensing Applications at Mid-Infrared Frequencies", *IEEE Photon. Technol. Lett.*, 30 (2018) 1917- 1920.

[27] I. Carvalho et al., "A Field-Enhancement Optical Fiber SPR Sensor Using Graphene, Molybdenum

Disulfide, and Zinc Oxide", *Plasmonics*, 18 (2023) 1705-1713.
[28] N.S. Sultan and O.A. Ali, "Study of the sensitivity of carbon quantum dots for NO_2 gas sensor and improve it using graphene", *Iraqi J. Phys.*, 22(4) (2024) 130-138.
[29] E.X. Perez, "Design, Fabrication and Characterization of Porous Silicon Multilayer Optical Devices", Ph.D thesis, University of Tarragona, Spain (2007).
[30] M.H. Nida and S.S. Al-Bassam, "Coreless optical fiber for hemoglobin (HB) sensing with bilayer based on surface plasmon resonance", *J. Opt.*, (2022), doi: 10.21203/rs.3.rs-1687798/v1.
[31] R. Jha et al., "Label-Free Biochemical Sensing Using Processed Optical Fiber Interferometry: A Review", *ACS Omega*, 9(3) (2024) 3037-3069.
[32] G.M. Jassam and S.S. Ahmed, "High sensitivity for toxic metal ion sensor based on tapered PCF Mach–Zehnder interferometer", *J. Opt.*, 53 (2023) 1079-1085.
[33] G.M. Jassam and S.S. Ahmed, "Tapered PCF Mach–Zehnder interferometer based on surface plasmon resonance (SPR) for estimating concentration toxic metal ions (lead)", *J. Opt.*, (2023), doi: 10.21203/rs.3.rs-1702252/v1.
[34] U. Afzal et al. "Fabrication of graphene-based sensor for exposure to different chemicals", *RSC Adv.,* (2022), doi: 10.1039/D2RA04776D.
[35] J.C. Santos-Ceballos et al., "Electrochemical modification of laser-induced graphene (LIG) with polyaniline (PANI) for ammonia sensing", *Sensors*, 25(18) (2025) 333-334.
[36] C. Walleni et al., "Selective NO_2 Gas Sensors Employing Nitrogen- and Boron-Doped and Codoped Reduced Graphene Oxide", *ACS Omega*, 9 (2024) 13028-13040.

Table (1) Properties and parameters of the Nano-Graphene chemical sensor [24,25]

Parameter/Property	Symbol	Description / Typical Value
Structure Type	—	Single-layer, few-layer, Nano-ribbon, Nano-mesh
Surface Area	A_S	2630 m{m}^2/{g}
Thickness	Th	1 atom / 0.34 nm for monolayer
Sensitivity	S	2–10%/ppm (depends on analyte and structure)
Selectivity Enhancers	—	Doping (N, metals), hybrid composites
Defect Density	n_d	Tunable; higher density in Nano-mesh, edge-rich
Conductivity	σ	~10^5 S/m (pristine graphene)
Carrier Mobility	μ	Up to 2×10^5 cm /V·s
Response Time	T_r	Few seconds to sub-second
Recovery Time	T_{rec}	Seconds to minutes
Functionalization	—	DNA, metal oxides, polymers, nanoparticles

Table (2) Summary of the Graphene chemical sensors applications [28-32]

Application	Structure/Modification	Target Analyte	Sensing Mechanism
Ammonia Detection	PPy/Graphene hybrid	NH_3	Chemiresistive
Hydrogen Detection	ZnO nanostructures/Graphene	H_2	Heterojunction/p-n
Nitrate Detection	Graphene Optical Fiber	NO_3^-	Optical/Absorptive
Chemical Warfare Agent	GO composites, Nafion/Graphene	DMMP, TMP, TIP	H-bonding/Electrochemical
Enzyme/Catalytic Sensors	Graphene/AuNP/enzyme hybrids	Glucose, H_2O_2	Electrochemical/Amperometric

Table (3) Summary of recent related literature focused on the subject of nano-graphene based chemical sensors

Year	Author et al.	Employed Model	Applications	Contribution	Gaps & Limitations
2022	Afzal et al.	Graphene thin-film opto-chemical sensor	VOC detection (IPA, acetone, toluene)	High sensitivity and sharp response and recovery times in optical detection of chemicals	Limited to optical modes, needs optimization for gas selectivity
2024	Walleni et al.	NiO nanoparticle decorated N-rGO nanohybrid	NO_2 gas sensing with high selectivity	Ultra-high sensitivity (5 orders of magnitude improvement) and very low LOD (<1 ppb)	Operates at elevated temperatures; scalability not addressed
2024	Serban et al.	Quaternary nanohybrid (CNHox-GO-SnO_2-PVP) resistive sensor	Ethanol vapor sensing	Enhanced sensitivity and cost-effective environmentally friendly sensor design	Humidity and long-term stability need study
2024	Vafaei et al.	UV-enhanced CVD graphene/TiO_2 chemi-resistive sensor	NO_2 gas sensing in air quality monitoring	Low-power operation, high sensitivity at low gas concentration	Balance of photoinduced adsorption/desorption needs further study
2025	Santos-Ceballos et al.	PANI@LIG chemo-resistive nanocomposite	Ammonia gas sensing, environmental monitoring	Low-cost, flexible gas sensor with ppb-level LOD and suitable for real conditions	Selectivity and humidity interference issues remain

Table (4) Laboratory method statement, experimental repetition details, and procedural accuracy for fiber treatment and graphene control

Experimental Element	Detailed Description	Replication & Reproducibility Notes
Etching Chemical Composition	66% HF and 33% distilled water (3:1 HF:H_2O)	Precise acid ratio disclosed, enabling accurate chemical duplication
Acid Application Method	Acid applied using a precision plastic micro-needle directly onto selected fiber core areas	Localized and controllable delivery of HF ensures targeted etching
Etching Conditions	Process conducted at room temperature (~25°C); no external heating	Eliminates thermal variables, improving replication between laboratories
Agitation / Stirring Conditions	The HF solution applied without mechanical agitation; natural wetting diffusion controls reaction	Eliminates variability from induced turbulence
Graphene Layer Control	Thickness controlled by etching duration and acid exposure	Allows replication through adjustment of time rather than uncontrolled deposition
Etching Duration	Exposure followed by a 10-minute chemical reaction period	Defines time-dependent etching depth and graphene interface conditions
Post-Etching Neutralization	Acid removed and fibers submerged in distilled water	Ensures reaction termination and fiber stability
Water Exchange Frequency	Distilled water replaced three times during rinse cycle	Ensures complete removal of HF and prevents post-reaction continuation
Temperature Stability	Entire procedure conducted under consistent ambient temperature ~25°C	Ensures uniform reaction rates and minimizes thermal fluctuation inconsistencies
Replication Likelihood	High — procedure explicitly quantifies materials, timing, temperature, application method	Enables repeatability across laboratories with minimal ambiguity

Table (5) The experimental performance metrics of the graphene sensors are presented

metal	Etching Time(min)	A graphene - layered	Sensitivity (Sn) [μm/RIU]	Signal to Noise Ratio (SNR)	Figure Of Merit (FOM)	Resolution [RIU]
Graphene	40min	8.39	16.451	0.031	5.06	6×10^{-5}
	60min	9.38	16.666	0.0085	14.28	6×10^{-5}

Table (6) The resonance wavelengths of graphene-based sensors corresponding to different ethanol concentrations and their associated refractive indices

Ethanol Concentration (%)	Refractive Index (RIU) -40min	Resonance wavelength λ_{res} (nm)-40 min	Refractive Index (RIU) -60 min	Resonance wavelength λ_{res} (nm)-60 min
10	1.3364	490	1.3406	560
15	1.3406	560	1.3418	580
20	1.3434	608	1.3424	590
25	1.3466	660	1.3427	595
30	1.3496	710	1.343	600

Table (7) Quantitative linear regression and correlation analysis

Sensor	Linear Fit (λ vs RI)	Slope (nm/RIU)	R^2	p-value	Interpretation
40 min taper	λ = 16667·RI – 21784	16667	0.99995	1.43×10^{-7}	Extremely strong positive linear relation
60 min taper	λ = 16667·RI – 21783	16667	0.999999	1.20×10^{-30}	Perfect linear correlation

Table (8) Calculated sensitivity from empirical data.

Sensor	Δλ (nm)	ΔRI (RIU)	Computed Sensitivity (nm/RIU)	Reported Sensitivity (μm/RIU)
40 min	710 – 490 = 220	1.3496 – 1.3364 = 0.0132	16666.7	16.451
60 min	600 – 560 = 40	1.3430 – 1.3406 = 0.0024	16666.7	16.666

